Effect of the Coulomb interaction on the gap in monolayer and bilayer graphene

Andreas Sinner and Klaus Ziegler
Institute for Physics, University of Augsburg, D-86135 Augsburg, Germany
(Received 10 May 2010; revised manuscript received 1 October 2010; published 29 October 2010)

We study effects of a repulsive Coulomb interaction on the spectral gap in monolayer and bilayer graphene in the vicinity of the charge neutrality point by employing the functional renormalization-group technique. In both cases Coulomb interaction supports the gap once it is open. For monolayer graphene we correctly reproduce results obtained previously by several authors, e.g., an apparent logarithmic divergence of the Fermi velocity and the gap as well as a fixed point corresponding to a quantum phase transition at infinitely large Coulomb interaction. On the other hand, we show that the gap introduces an additional length scale at which renormalization flow of diverging quantities saturates. An analogous analysis is also performed for bilayer graphene with similar results. We find an additional fixed point in the gapless regime with linear spectrum corresponding to the vanishing electronic band mass. This fixed point is unstable with respect to gap fluctuations and cannot be reached as soon as the gap is opened. This preserves the quadratic scaling of the spectrum and finite electronic band mass.

DOI: 10.1103/PhysRevB.82.165453 PACS number(s): 71.10.−w, 05.10.Cc

I. INTRODUCTION

Monolayer (ML) and bilayer (BL) graphene are semimetals with an electron and a hole band. Both bands touch each other at two nodes. The low-energy dispersion in the vicinity of these nodes is linear in ML graphene and quadratic in BL graphene. Exactly at the nodes both systems obey a chiral symmetry which reflects the sublattice symmetry of the underlying honeycomb lattice for ML or the inversion symmetry between single layers for BL. These symmetries can be broken, either by adding hydrogen atoms to ML graphene[1–3] or by a biased gate voltage applied to BL graphene.[4] The symmetry breaking is accompanied by opening of a gap in the spectrum. Then the question is whether or not such a gap is suppressed or supported by the Coulomb interaction. Previous studies have shown that disorder induces random fluctuations of the gap which can suppress the effective gap and allow ML and BL graphene to be a conductor and to have a metal-insulator transition for a sufficiently large average gap.[5,6] On the other hand, it has been discussed that a short-range (Gross-Neveu) electron-electron interaction can dominate the long-range Coulomb interaction, leading eventually to an insulating behavior.[7] In contrast to this works, we will follow subsequently a more direct route to an insulator by assuming a small gap and study how this is affected by the Coulomb interaction itself. The problem of Coulomb interaction in graphene has been previously studied by employing a perturbative renormalization-group (RG) approach, for clean ML graphene[7–13] as well as for disordered ML graphene.[14–16] These studies show clearly a strong renormalization of the Fermi velocity in the clean case and considerable interplay between Coulomb interaction and disorder.

The outline of this paper is as follows. In Sec. II we define the effective-field theory for both graphene configurations with Coulomb interaction. We introduce the gap into the action by hand and perform decoupling in the interaction channel by means of the Hubbard-Stratonovich transformation. We obtain expressions for the bare bosonic and fermionic propagators and interaction vertices. In Sec. III we write down renormalization-group flow equations for the gap parameter and fermionic wave-function renormalization factors and solve them for both gapless and gapped regimes. Furthermore, we analyze the fixed points (FPs) for both graphene configurations.

II. MODEL

We start with the zero-temperature model for gapped ML and BL graphene. In the real space the Euclidean action of noninteracting ML and BL graphene in vicinity of a nodal point is given by

$$\mathcal{S}_0[\psi^\dagger,\psi] = -\int_X \psi_X^\dagger(\hbar\partial_t - i\vec{\tau}\cdot\vec{\nabla} + \Delta_0\tau_3)\psi_X. \tag{1}$$

Here, Grassman fields $\psi^{\mathrm{T}}=(\psi_{AK},\psi_{BK},\psi_{BK'},\psi_{AK'})$ represent four-component spinors on the sublattices A and B in the vicinity of nodal points K and K′ in the momentum space which depend on the $2+1$-dimensional vector X that contains imaginary time t and spatial vector $\vec{x}$ as components. Matrices $\tau_{i,3}=\mathbb{1}\otimes\sigma_{i,3}$, $i=1,2$, where $\sigma_{i,3}$ denote usual Pauli matrices. For ML graphene the operator $\vec{\nabla}$ reads

$$\vec{\nabla} = \hbar v\partial_{\vec{x}}, \tag{2}$$

where $v=\sqrt{3}ta/2\hbar$ denotes the bare (nonrenormalized) Fermi velocity and $\partial_{\vec{x}}$ usual differential operators. For BL graphene it has the components,

$$\nabla_1 = \frac{\hbar^2}{2\mu i}(\partial_{x_1}^2 - \partial_{x_2}^2), \tag{3}$$

$$\nabla_2 = \frac{\hbar^2}{2\mu i}2\partial_{x_1}\partial_{x_2} \tag{4}$$

with the bare band mass of electrons defined as

$$\mu = \frac{2t_\perp \hbar^2}{3t^2 a^2}.$$

Here, t and $t_\perp$ are in- and out-of-plane hopping energies, respectively; a denotes the lattice spacing. The spectral gap Δ_0 is simply introduced by hand. The instantaneous Coulomb interaction is the same for both graphene configurations,

$$\mathcal{S}_c[\psi^\dagger,\psi] = \frac{\hbar g}{2}\int_X \int_{X'} (\psi^\dagger\psi)_X \frac{\delta(t-t')}{|\vec{x}-\vec{x}'|}(\psi^\dagger\psi)_{X'}. \quad (5)$$

The microscopic strength of the Coulomb interaction between electrons is given by

$$g = \frac{e^2}{8\pi\epsilon_0\epsilon\hbar} = \frac{\alpha c}{2\epsilon},$$

where e denotes the elementary charge, ϵ_0 the dielectric constant of the vacuum, α the fine structure constant, c the speed of light in vacuum, and ϵ the relative dielectric constant of the substrate. After performing a Fourier transform we obtain for both configurations

$$\mathcal{S}[\psi^\dagger,\psi] = -\int_Q \psi_Q^\dagger[i\hbar q_0 + \vec{h}\cdot\vec{\tau} + \Delta_0\tau_3]\psi_Q + \frac{\hbar g'}{2}\int_Q \frac{1}{q}\rho_Q\rho_{-Q} \quad (6)$$

with different kinetic-energy parts. The integrals over momentum and frequency $Q=(q_0,\vec{q})$ with the absolute value of the momentum q and zero-temperature Matsubara frequency q_0 read $\int_Q = (2\pi)^{-3}\int dq_0 d^2\vec{q}$ and should be thought of being regularized by means of an UV cutoff Λ_0. Furthermore we have rescaled the interaction strength by the factor 2π that appears after Fourier transform, introducing $g'=2\pi g$. The fermionic densities are defined as

$$\rho_Q = \int_P \psi_P^\dagger \psi_{P+Q}.$$

For ML graphene the components of the vector $\vec{h}$ in the noninteracting part of the action read

$$h_i = \hbar v q_i \quad (7a)$$

while for BL graphene

$$h_1 = \frac{\hbar^2}{2\mu}(q_1^2 - q_2^2), \quad h_2 = \frac{\hbar^2}{\mu}q_1 q_2. \quad (7b)$$

Below we will assume $\hbar = 1$.

Now we map the pure fermionic action, Eq. (6), onto the action containing both fermionic and bosonic degrees of freedom by means of the Hubbard-Stratonovich transformation,[17]

$$\mathcal{S}_0[\psi^\dagger,\psi] + \mathcal{S}_c[\psi^\dagger,\psi] \to \mathcal{S}_0[\psi^\dagger,\psi] + \mathcal{S}_0[\phi] + \mathcal{S}_Y[\psi^\dagger,\psi,\phi], \quad (8)$$

where the free-bosonic action reads

$$\mathcal{S}_0[\phi] = \frac{1}{2g'}\int_Q q\phi_Q\phi_{-Q} \quad (9)$$

and the third term denotes the interacting Yukawa term describing coupling between fermions and bosons,

$$\mathcal{S}_Y[\psi^\dagger,\psi,\phi] = i\int_Q \int_K \psi_K^\dagger \psi_{K+Q}\phi_{-Q}. \quad (10)$$

From the mixed action, Eq. (8), we obtain vertices and propagators by taking functional derivatives with respect to each field. From

$$\left.\frac{\delta^2\mathcal{S}}{\delta\psi_Q\delta\psi_{Q'}^\dagger}\right|_{\psi^\dagger,\psi,\phi=0} = -(2\pi)^3\delta_{Q,Q'}G_0^{-1}(Q), \quad (11)$$

we obtain the inverse fermionic propagator

$$G_0^{-1}(Q) = iq_0 + \vec{h}\cdot\vec{\tau} + \Delta_0\tau_3 \quad (12)$$

with components of the vector $\vec{h}$ defined in Eqs. (7a) and (7b), and from

$$\left.\frac{\delta^2\mathcal{S}}{\delta\phi_Q\delta\phi_{Q'}}\right|_{\psi^\dagger,\psi,\phi=0} = -(2\pi)^3\delta_{Q,-Q'}F^{-1}(Q), \quad (13)$$

the inverse bosonic propagator

$$F^{-1}(Q) = -\frac{q}{g'}. \quad (14)$$

Finally, the bare Yukawa vertex is obtained as

$$\Gamma(P_1;P_2,P_3) = \left.\frac{\delta^3\mathcal{S}}{\delta\psi_{P_1}\delta\psi_{P_2}^\dagger\delta\phi_{P_3}}\right|_{\psi^\dagger,\psi,\phi=0}. \quad (15)$$

We arrive at

$$\Gamma(P_1;P_2,P_3) = i(2\pi)^3\delta_{P_1,P_2+P_3}. \quad (16)$$

III. RENORMALIZATION-GROUP EQUATIONS

The functional RG is conveniently defined in terms of the field-dependent functional of effective action $\mathcal{L}[\Phi]$, which in turn represents the Legendre transform of the generating functional of connected Green's functions. For our purposes the ensemble average field $\Phi=(\bar{\psi},\bar{\psi}^\dagger,\bar{\phi})$ is supposed to contain both fermionic and bosonic entries.[17] The functional $\mathcal{L}$ depends on the IR cutoff $\Lambda\leq\Lambda_0$, which is eventually removed. The derivation of the functional RG flow equation is described in detail in Refs. 17–20. The RG flow of $\mathcal{L}$ is generated by the regulator function introduced into the propagator of the noninteracting system and is determined by

$$\partial_\Lambda\mathcal{L}_\Lambda[\Phi] = -\frac{1}{2}\mathrm{Tr}\left\{\partial_\Lambda[G_{0,R_\Lambda}^{-1}]\left(\frac{\delta^2\mathcal{L}_\Lambda^R}{\delta\Phi\,\delta\Phi}[\Phi]\right)^{-1}\right\}, \quad (17)$$

where $[G_{0,R_\Lambda}^{-1}]$ is the propagator of the noninteracting system depending on the cutoff Λ only via the regulator function. The matrix

$$\left.\frac{\delta^2\mathcal{L}_\Lambda^R}{\delta\Phi\,\delta\Phi}[\Phi]\right|_{\Phi=0} = -[G_\Lambda^R]^{-1} = -([G_{0,R_\Lambda}^{-1}] - \Sigma_\Lambda) \tag{18}$$

denotes the regularized full inverse propagator with Σ_Λ meaning the irreducible self-energy. The choice of the regulator will be specified a few lines below. Note that all quantities which appear on the right-hand side of Eq. (17) dwell on the space of composite fields Φ and therefore represent 3×3 matrices.

Since our main interest is the determination of the spectrum renormalization of fermions due to the Coulomb interaction, we will focus on the coupling parameters in the fermionic sector of the theory. In the simplest approximation we make the following ansatz for the running effective action:

$$\mathcal{L}_\Lambda[\Phi] \approx -\int_Q \bar{\psi}_Q^\dagger [iq_0 + Z_\Lambda^{-1}\vec{h}\cdot\vec{\tau} + \Delta_\Lambda\tau_3]\bar{\psi}_Q - \frac{1}{2}\int_Q F^{-1}(Q)\bar{\phi}_Q\bar{\phi}_{-Q} + i\int_Q\int_K \bar{\psi}_Q^\dagger\bar{\psi}_{Q+K}\bar{\phi}_{-K}, \tag{19}$$

which takes only the renormalization of the energy gap and of the electronic dispersion into account. We do not consider the renormalization of the Matsubara frequency since we assume the Coulomb interaction to be absolutely instantaneous. The inverse bosonic propagator $F^{-1}(Q)$ is defined in Eq. (14). For momenta larger than the UV cutoff Λ_0 the action in Eq. (19) must reproduce the bare action from Eq. (8). Therefore the initial conditions are chosen as $Z_{\Lambda_0}=1$ and $\Delta_{\Lambda_0}=\Delta_0$.

Taking functional derivatives with respect to both Grassmanian fields on both sides of Eq. (17) and putting subsequently $\Phi=0$ we arrive at the RG flow equation for the inverse renormalized fermionic propagator. For details of its derivation we refer to Refs. 17 and 18. If we employ the regularization scheme with the regulator built in the fermionic lines only, this equation can be written in the following algebraic form (note an additional minus sign due to Fermi statistics):

$$\partial_\Lambda G_\Lambda^{-1}(Q) = \int_P \dot{G}_\Lambda(P)F(P-Q), \tag{20}$$

where $F(Q)$ is the bare Coulomb potential defined in Eq. (14), and the single scale propagator $\dot{G}_\Lambda$ is defined as

$$\dot{G}_\Lambda = -G_\Lambda^R\partial_\Lambda[G_{0,R_\Lambda}^{-1}]G_\Lambda^R. \tag{21}$$

We will work within the so-called sharp cutoff regularization scheme.[20] Then the momentum cutoff is introduced as follows:

$$G_{0,R_\Lambda}(Q) = \Theta(\Lambda < q < \Lambda_0)G_0(Q), \tag{22}$$

where $\Theta(\Lambda<q<\Lambda_0)=\Theta(\Lambda_0-q)-\Theta(\Lambda-q)\to\Theta(q-\Lambda)$ as $\Lambda_0\to\infty$. For momenta smaller than the UV cutoff Λ_0, the flowing fermionic propagator $G_\Lambda^R(Q)$ is

$$G_\Lambda^R(Q) = -\Theta(q-\Lambda)\frac{iq_0 - Z_\Lambda^{-1}\vec{h}\cdot\vec{\tau} - \Delta_\Lambda\tau_3}{q_0^2 + E_\Lambda^2(q)}, \tag{23}$$

and hence the single-scale propagator[20]

$$\dot{G}_\Lambda(Q) = \delta(q-\Lambda)\frac{iq_0 - Z_\Lambda^{-1}\vec{h}\cdot\vec{\tau} - \Delta_\Lambda\tau_3}{q_0^2 + E_\Lambda^2(q)}, \tag{24}$$

where we have introduced $E_\Lambda(q)=\sqrt{\Delta_\Lambda^2+\epsilon_\Lambda^2(q)}$ with the renormalized spectra of free fermions $\epsilon_\Lambda(q)=Z_\Lambda^{-1}vq$ for ML and $\epsilon_\Lambda(q)=(2\mu Z_\Lambda)^{-1}q^2$ for BL. For both ML and BL the flow equations for the coupling parameter Δ_Λ is extracted from Eq. (20) in the same way,

$$\partial_\Lambda\Delta_\Lambda = \frac{1}{4}\mathrm{Tr}_2\{\tau_3\partial_\Lambda G_\Lambda^{-1}(Q)\}|_{Q=0}, \tag{25a}$$

where Tr_2 denotes a trace operator acting on the pseudospin and valley space only. The RG flow equations for the factor Z_Λ are extracted differently for ML and BL due to the different scaling of the spectra in these configurations,

$$\mathrm{ML}:\partial_\Lambda Z_\Lambda^{-1} = \frac{1}{4v}\frac{\partial}{\partial q_i}\mathrm{Tr}_2\{\tau_i\partial_\Lambda G_\Lambda^{-1}(Q)\}|_{Q=0}, \tag{25b}$$

$$\mathrm{BL}:\partial_\Lambda Z_\Lambda^{-1} = \frac{\mu}{4}\frac{\partial^2}{\partial q_1^2}\mathrm{Tr}_2\{\tau_1\partial_\Lambda G_\Lambda^{-1}(Q)\}|_{Q=0}, \tag{25c}$$

for $i=1,2$.[21] Introducing the logarithmic flow parameter $\ell=\log(\Lambda_0/\Lambda)$ we obtain the same flow equation for the gap for both graphene configurations

$$\partial_\ell\Delta_\ell = \frac{\bar{g}\Delta_\ell\Lambda}{\sqrt{\Delta_\ell^2+\epsilon_\ell^2}}, \tag{26a}$$

where $\bar{g}=g'/4\pi$ but different equations for the wave-function renormalization factor,

$$\mathrm{ML}:\partial_\ell Z_\ell = -\frac{1}{2}\frac{\bar{g}Z_\ell\Lambda}{\sqrt{\Delta_\ell^2+\epsilon_\ell^2}}, \tag{26b}$$

$$\mathrm{BL}:\partial_\ell Z_\ell = -\frac{3}{8}\frac{\bar{g}Z_\ell\Lambda}{\sqrt{\Delta_\ell^2+\epsilon_\ell^2}}. \tag{26c}$$

Here we have used the identity $\partial_\ell Z_\ell^{-1}=-Z_\ell^{-2}\partial_\ell Z_\ell$. The flowing free-fermion spectra are

$$\mathrm{ML}:\epsilon_\ell = vZ_\ell^{-1}\Lambda, \tag{27a}$$

$$\mathrm{BL}:\epsilon_\ell = (2\mu Z_\ell)^{-1}\Lambda^2. \tag{27b}$$

The scaling dimension of the energy (i.e., the dynamical exponent) is defined as $z=1-\eta_\ell$ for ML and $z=2-\eta_\ell$ for BL. Here, η_ℓ is referred to as the anomalous dimension which can be obtained from the parameter Z_ℓ by

$$\eta_\ell = -\partial_\ell \log Z_\ell. \tag{28}$$

Below we discuss solutions of these equations in gapless and gapped regimes.

A. Gapless regime

In the gapless regime Eqs. (26a)–(26c) are easily solved. The only solution of Eq. (26a) is the trivial one $\Delta_\ell=\Delta_{\ell=0}=0$ while Eqs. (26b) and (26c) reduce to

$$\partial_\ell Z_\ell^{-1}=\lambda_{\mathrm{ML}}$$

with $\lambda_{\mathrm{ML}}=\bar{g}/(2v)$ for ML and correspondingly

$$\partial_\ell Z_\ell^{-1}=\lambda_{\mathrm{BL}}e^{\ell}$$

with $\lambda_{\mathrm{BL}}=3\mu\bar{g}/(4\Lambda_0)$ for BL with solutions,

$$\mathrm{ML}: Z_\ell^{-1}=1+\lambda_{\mathrm{ML}}\ell, \tag{29}$$

$$\mathrm{BL}: Z_\ell^{-1}=1-\lambda_{\mathrm{BL}}+\lambda_{\mathrm{BL}}e^{\ell}. \tag{30}$$

The result of Eq. (29) corresponds to the well-known logarithmic renormalization of the Fermi velocity $v_\ell=Z_\ell^{-1}v$ in clean ML graphene due to the Coulomb interaction.[8–11,22] Similarly, Eq. (30) describes the renormalization of the electronic band mass $\mu_\ell=Z_\ell\mu$ in BL. At small momenta the band mass decreases proportionally to the momentum $\mu_\ell\propto\Lambda$, i.e., the particles become effectively faster in analogy to ML. Using Eq. (28) we obtain expressions for the anomalous dimension

$$\mathrm{ML}: \eta_\ell=\lambda_{\mathrm{ML}}Z_\ell, \tag{31a}$$

$$\mathrm{BL}: \eta_\ell=\lambda_{\mathrm{BL}}Z_\ell e^{\ell}. \tag{31b}$$

For $\ell\to 0$ Eq. (31a) approaches zero, meaning that the scaling dimension of the energy in ML remains $z=1$ and nothing changes the relativistic behavior of electrons. In contrast, Eq. (31b) approaches in this limit unity. This means that the scaling dimension of the energy $z=2-\eta_\ell$ becomes relativistic in BL with the velocity $v_s=3\bar{g}/8$, i.e., in vacuum $c/v_s\approx 1450$. Therefore, in absence of a gap in the spectrum of BL the Coulomb interaction attempts to linearize the fermionic dispersion in vicinity of the nodal points. Similar conclusions have been recently made by Kusminskiy *et al.*[23] for finite values of chemical potential. Their findings provided a good explanation of recent cyclotron experiments,[24] where the effects discussed here have been observed.

An estimation for the suitable scale below which this effect is observable can be made as follows: the only scale which affects the flow of the band mass in gapless BL graphene can be read off from Eq. (30) (cf. Fig. 4),

$$\ell' \approx \log\left(\frac{1-\lambda_{\mathrm{BL}}}{\lambda_{\mathrm{BL}}}\right). \tag{32}$$

Choosing Λ_0 to be equal to the inverse lattice spacing we find for a realistic experimental situation ($\epsilon=1-4$) $\ell'\approx 2.3-3.8$ and the corresponding momentum scale to be of the order $k_c=\Lambda_0 e^{-\ell'}\approx 1\times 10^{-2}-7\times 10^{-2}$ Å^{-1}.

B. Gapped regime

Naively, for $\Delta_\ell\ll\epsilon_\ell$ we can neglect Δ_ℓ in the denominator. For ML we obtain from Eqs. (26a)

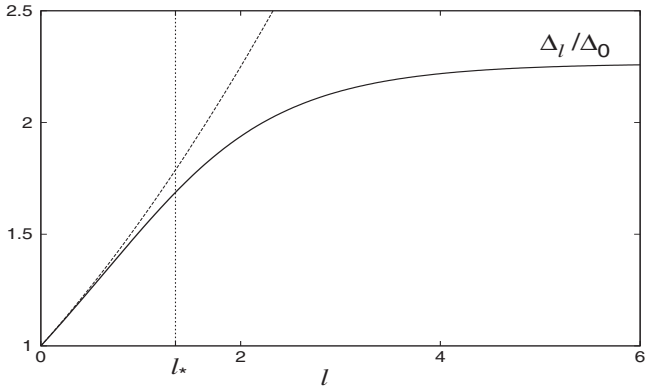

FIG. 1. Renormalization of the gap Δ_ℓ in ML because of Coulomb interaction. The crossover scale ℓ_* is determined from Eq. (35). The initial value of the gap is $\Delta_0=0.2v_0\Lambda_0$, the dielectric constant $\epsilon=1$. The dashed line shows the Kane/Mele asymptote from Eq. (34). The crossover scale ℓ_* is determined from Eq. (35).

$$\partial_\ell \log\Delta_\ell=2\lambda_{\mathrm{ML}}Z_\ell, \tag{33}$$

which together with Eq. (29) reproduces the Kane/Mele result,[12]

$$\Delta_\ell=\Delta_0(1+\lambda_{\mathrm{ML}}\ell)^2=\Delta_0 Z_\ell^{-2} \tag{34}$$

with the apparently logarithmically diverging gap. However, Eq. (34) suggests that at large ℓ denominators in Eqs. (26a) and (26b) are dominated by the gap, i.e., $E_{\ell\gg\ell_*}=\sqrt{\Delta_\ell^2+\epsilon_\ell^2}\sim\Delta_\ell$, where the crossover scale ℓ_* can be determined from the condition

$$\Delta_{\ell_*}\approx\epsilon_{\ell_*}, \tag{35}$$

which turns out to be a nonlinear algebraic equation if we take Eqs. (27a), (29), and (33) into account. However, Eq. (35) can be uniquely solved numerically. The solution of Eq. (26a) in this case becomes

$$\Delta_\ell\approx\Delta_{\ell_*}+\bar{g}\Lambda_*(1-e^{-\ell}). \tag{36}$$

The physical gap is obtained for $\ell\to\infty$

$$\Delta_c=\Delta_*+\bar{g}\Lambda_*\approx\epsilon_*+\bar{g}\Lambda_*. \tag{37}$$

Therefore the Coulomb interaction in ML supports the gap once it is opened, independently of the bare gap magnitude. A typical flow of the gap parameter in ML is shown in Fig. 1. At the same scale the logarithmic growth of the Fermi velocity stops and it also stabilizes at the finite value $v_c\approx v\sqrt{1+\bar{g}\Lambda_*/\Delta_*}$ as depicted in Fig. 2.

The solutions for the gap in BL are similar in spirit but with an extra fixed point. For $\Delta_\ell\ll\epsilon_\ell$ we obtain

$$\Delta_\ell=\Delta_0 Z_\ell^{-8/3} \tag{38}$$

and therefore $\Delta_{\ell\to\infty}\to\infty$. The solution for $\Delta_\ell\gg\epsilon_\ell$ is formally given by Eq. (36), too, such that the flow of the gap stabilizes at some finite value Δ_* (cf. Fig. 3). On the other hand, the presence of the gap stabilizes the flow of the wave function renormalization factor Z_ℓ and therefore the flow of the electronic band mass $\mu_\ell=\mu_0 Z_\ell$, which in this case remains finite

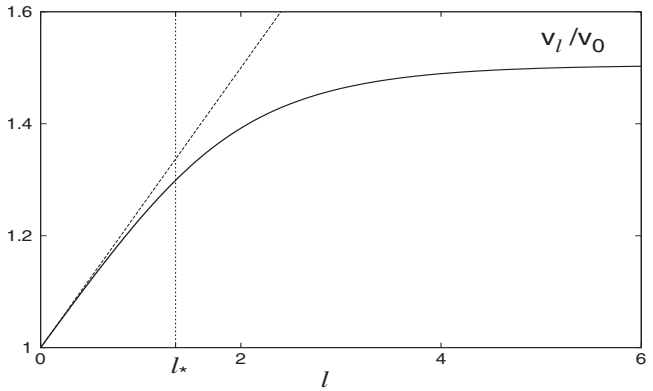

FIG. 2. Renormalization of the Fermi velocity $v_\ell = v_0 Z_\ell^{-1}$ in ML because of Coulomb interaction with [solid line, full solutions of Eqs. (26a) and (26b)] and without a gap [dashed line, Eq. (29)]. The crossover scale ℓ_* is determined from Eq. (35).

(cf. Fig. 4). The scaling of the kinetic energy is in this case also preserved and remains equal to 2.

In order to shed some light on the topological properties of the RG flow in the parametric space it is convenient to redefine Eqs. (26b) and (26c) in terms of kinetic energy and introduce dimensionless parameters by expressing both the gap and kinetic energy in units of Coulomb energy,

$$\bar{\Delta}_\ell = \frac{\Delta_\ell}{\bar{g}\Lambda}, \tag{39a}$$

$$\bar{\epsilon}_\ell = \frac{\epsilon_\ell}{\bar{g}\Lambda} \tag{39b}$$

with ϵ_ℓ defined in Eq. (27a) for ML and in Eq. (27a) for BL. For both ML and BL we arrive at the same equation for the rescaled gap

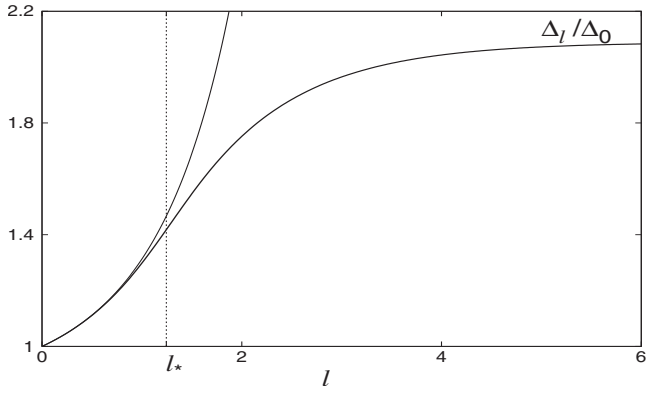

FIG. 3. Renormalization of the gap Δ_ℓ in BL because of Coulomb interaction. The crossover scale ℓ_* is determined from Eq. (35). The initial value of the gap is $\Delta_0 = 0.2 v_0 \Lambda_0$, the dielectric constant $\epsilon = 1$. The dashed line shows the large kinetic-energy asymptote from Eq. (38). The crossover scale ℓ_* is determined from Eq. (35).

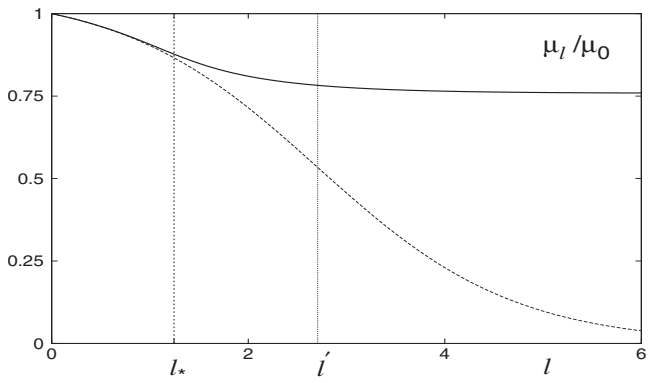

FIG. 4. The renormalization of the band mass $\mu_\ell = \mu_0 Z_\ell$ due to the Coulomb interaction. The solid line shows the flow of the band mass of BL graphene with a gap. Dashed line shows asymptotic renormalization without a gap. In this case the electronic band mass scales to zero. This leads to the linear scaling of the spectrum. The scale ℓ' is found from Eq. (32).

$$\partial_\ell \bar{\Delta}_\ell = \bar{\Delta}_\ell + \frac{\bar{\Delta}_\ell}{\sqrt{\bar{\epsilon}_\ell^2 + \bar{\Delta}_\ell^2}} \tag{40a}$$

while equations for the rescaled kinetic energy are different due to different scaling behavior of spectra,

$$\text{ML:} \partial_\ell \bar{\epsilon}_\ell = \frac{1}{2} \frac{\bar{\epsilon}_\ell}{\sqrt{\bar{\epsilon}_\ell^2 + \bar{\Delta}_\ell^2}}, \tag{40b}$$

$$\text{BL:} \partial_\ell \bar{\epsilon}_\ell = \frac{3}{8} \frac{\bar{\epsilon}_\ell}{\sqrt{\bar{\epsilon}_\ell^2 + \bar{\Delta}_\ell^2}} - \bar{\epsilon}_\ell. \tag{40c}$$

The flow in the parametric space is schematically shown in Fig. 5. The FPs are obtained by setting the right-hand sides of Eqs. (40a)–(40c) to zero and solving the emerging system of algebraic equations. For ML graphene the only instable fixed point is at both $\bar{\Delta}_\ell = 0$ and $\bar{\epsilon}_\ell = 0$. From Eq. (39b) follows that this fixed point can be reached if

$$\bar{\epsilon}_\ell = \frac{v Z_\ell^{-1}}{\bar{g}} \to 0. \tag{41}$$

Since Z_ℓ^{-1} flows to a finite value, this can only be satisfied if $\bar{g} \to \infty$. This is a case of the famous quantum phase transition discussed in Refs. 8 and 11. The instability of the fixed point means that the flow can leave it in every direction. For any

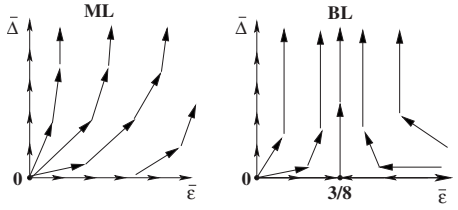

FIG. 5. Schematic RG flow for both graphene configurations in the space spanned by the dimensionless kinetic energy $\bar{\epsilon}_\ell$ and gap parameter $\bar{\Delta}_\ell$.

finite initial value of the gap it develops infinitely large value which indicates a finite physical gap. In contrast to the ML graphene, there is a nontrivial fixed point at finite dimensionless kinetic energy $\bar{\epsilon}_*=3/8$ in the case of gapless BL graphene. This fixed point is characterized by the anomalous scaling dimension $\eta_\ell=1$, i.e., the spectrum of BL becomes in this case linear. However this fixed point is instable with respect to the finite gap direction, i.e., once a small gap is opened in the spectrum the flow cannot reach this fixed point anymore but runs toward an infinite value. On the other hand, since the numerical value of $\bar{\epsilon}_*$ at this fixed point suggests a strong-coupling regime we might need to go beyond the truncation, Eq. (19), and take additionally flow of the $\bar{\psi}\bar{\psi}^\dagger\bar{\phi}$—vertex into account.

IV. CONCLUSIONS

In conclusion, we have studied both ML and BL graphene with Coulomb interaction and a uniform gap by employing a renormalization-group technique. In contrast to previous approaches to gapped ML graphene based on the renormalization-group approach,[7,9,11,12] which predict logarithmically divergent renormalization of the gap and the Fermi velocity, our results suggest a saturation of RG flows at an intrinsic scale related to the gap. This saturation takes place for both ML and BL graphene, for any finite initial value of the gap no matter how small it is, and since measured quantities should be finite, this might be suggestive of a gap in the spectrum of both configurations at energies below 0.1 eV.

In ML graphene the Coulomb energy exhibits the same scaling as the kinetic energy. Once a spectral gap is opened it creates an additional length scale which dominates the physics at small momenta. This scale cuts off the logarithmic divergence of the Fermi velocity and gap itself such that the flow of both quantities stabilizes at the finite value.

For gapless BL graphene is shown that Coulomb interaction renormalizes the electronic band mass which scales to zero for small momenta. This leads to a paradoxical result that the electronic spectrum should become linear close to the charge neutrality point. This regime corresponds to a stable fixed point and therefore the flow should inevitably go into this point. The quadratic scaling of the spectrum is rescued by the presence of the gap since for any finite starting values of the gap the flow of the band mass always saturates at a finite value.

ACKNOWLEDGMENTS

We gratefully acknowledge useful discussions with S. Savel'ev, B. Dóra, and A. Sedrakyan. We thank A. H. Castro Neto for bringing Refs. 23 and 24 to our attention. This work has been supported by the DFG under Grant No. ZI 305/5-1.

[1] It should be mentioned that it is difficult to distinguish a genuine gap from the disorder generated localization near the nodal points in experimental situations.
[2] E. J. Duplock, M. Scheffler, and P. J. D. Lindan, Phys. Rev. Lett. **92**, 225502 (2004).
[3] D. C. Elias, R. R. Nair, T. M. G. Mohiuddin, S. V. Morozov, P. Blake, M. P. Halsall, A. C. Ferrari, D. W. Boukhvalov, M. I. Katsnelson, A. K. Geim, and K. S. Novoselov, Science **323**, 610 (2009).
[4] T. Ohta, A. Bostwick, T. Seyller, K. Horn, and E. Rotenberg, Science **313**, 951 (2006).
[5] K. Ziegler, Phys. Rev. Lett. **102**, 126802 (2009).
[6] K. Ziegler, Phys. Rev. B **79**, 195424 (2009).
[7] V. Juričić, I. F. Herbut, and G. W. Semenoff, Phys. Rev. B **80**, 081405(R) (2009).
[8] D. T. Son, Phys. Rev. B **75**, 235423 (2007).
[9] E. G. Mishchenko, Phys. Rev. Lett. **98**, 216801 (2007).
[10] E. G. Mishchenko, EPL **83**, 17005 (2008).
[11] D. E. Sheehy and J. Schmalian, Phys. Rev. Lett. **99**, 226803 (2007).
[12] C. L. Kane and E. J. Mele, Phys. Rev. Lett. **95**, 226801 (2005).
[13] J. E. Drut and T. A. Lähde, Phys. Rev. Lett. **102**, 026802 (2009).
[14] T. Stauber, F. Guinea, and M. A. H. Vozmediano, Phys. Rev. B **71**, 041406(R) (2005).
[15] M. S. Foster and I. L. Aleiner, Phys. Rev. B **77**, 195413 (2008).
[16] I. F. Herbut, V. Juričić, and O. Vafek, Phys. Rev. Lett. **100**, 046403 (2008).
[17] F. Schütz, L. Bartosch, and P. Kopietz, Phys. Rev. B **72**, 035107 (2005).
[18] F. Schütz and P. Kopietz, J. Phys. A **39**, 8205 (2006).
[19] C. Wetterich, Phys. Lett. B **301**, 90 (1993).
[20] T. R. Morris, Int. J. Mod. Phys. A **9**, 2411 (1994).
[21] The same flow equation for the wave renormalization factor Z_Λ for BL can be extracted in several ways because of the different components of the vector $\vec{h}$.
[22] J. González, F. Guinea, and M. A. H. Vozmediano, Phys. Rev. B **59**, R2474 (1999).
[23] S. V. Kusminskiy, D. K. Campbell, and A. H. Castro Neto, EPL **85**, 58005 (2009).
[24] E. A. Henriksen, Z. Jiang, L.-C. Tung, M. E. Schwartz, M. Takita, Y.-J. Wang, P. Kim, and H. L. Stormer, Phys. Rev. Lett. **100**, 087403 (2008).